Novel Material with Narrow-Band Transparency Window in the Bulk

Chryssoula A. Kyriazidou, *Member, IEEE*,, Rodolfo E. Diaz, and Nicólaos G. Alexópoulos, *Fellow, IEEE*

***Abstract*—This paper presents the theoretical design of an artificial dielectric exhibiting narrowband frequency selective properties in the bulk without relying on periodic placement of elements. In this manner, it initiates a novel approach that bypasses the drawbacks of the traditional frequency selective surfaces (FSS), namely, unwanted passbands, dependence on excitation angle and polarization, and difficulties in conversion from planar to curved geometries. The key design elements are the concentric geometry of the inclusions and the use of Lorentzian resonant media. A discussion of physical resonant materials is presented, substantiating the credibility of the theoretical design. To illustrate the approach, a novel complex medium is synthesized as an ensemble of spherical particles composed of a lossy core coated with a highly resonant dielectric layer and embedded into a dielectric host. The resulting structure is an amorphous substance, lossy over its entire spectrum except for two narrow-band transparency windows, where it may become as lossless as desired. The parameter space of the system is thoroughly analyzed which determines the type of constitutive materials and geometries for tailor-designing the windows according to specifications (shape, positioning and overall normalization). In this sense, the lossy concentric structure forms an ideal candidate for thin absorbing films (TAF's) with extensive applications in antenna systems, RF absorbers, and anechoic chambers.**

***Index Terms*—Artificial dielectric, frequency selective surfaces.**

I. Introduction

FREQUENCY selective surfaces (FSS) are periodic structures with bandfiltering characteristics, traditionally constructed either as periodically perforated metallic screens or as arrays of metallic patches printed on dielectric substrates. Applications range from the microwave region in multiband antenna systems, narrowband reflectors, radomes for active radar systems, RF absorbers [1]–[7], up to the far and near infrared portion of the spectrum as mirrors in molecular lasers, polarizers, and solar selective surfaces [8]–[10]. However, existing FSS suffer from three major drawbacks. First, the conversion from the desired design on a flat surface to the realistic curved surface of the typical application requires extensive empirical corrections. Second, because the surfaces use implanted elements comparable in size to the desired wavelength, they can exhibit unwanted passbands and grating lobe scattering at out-of-band frequencies. Third, filtering characteristics vary with incidence angle and polarization, requiring special stabilization designs. These drawbacks form the motivation for research into materials capable of exhibiting frequency selective properties in the bulk without unwanted passbands or inherent limitation on their topology, for use in radomes, reflectors, or specialized space filters.

This paper initiates a novel approach whereby narrowband filtering properties are created from random composite structures based on the physical resonant properties of the constituents and the geometry of inclusions. In this manner, a bulk continuous material rather than a lattice formation is used to manipulate and shape the electromagnetic propagation. The novel artificial dielectrics constitute conformal FSS to be applied by means of a uniform coating process to simple planar or complex curvilinear shapes.

The approach is illustrated by a theoretical design for a random mixture with frequency selective properties, characterized by a concentric geometry for the inclusions. The frequency dispersion of the proposed composite is driven by the use of a Lorentzian resonant dielectric as one of the constituent media. The existence and availability of such resonant materials is essential for the physical realization of the proposed composite structures. This issue is discussed with an emphasis on the microwave regime, where the example of a physical resonant medium is given. Moreover, our particular model uses a lossy core for the implants, thus focusing on a lossy filtering composite medium, ideal for applications of thin absorbing films (TAF's). The use of dilute mixtures of small coated and uncoated metallic particles has been proposed in the past [11], but for broad-band frequency selection and with conventional nonresonant constituents.

Our design actually relies on the explanation of the optical transparency of water according to the analytic theory of dielectrics [12]. In that work, the extreme transparency window of water (eight orders of magnitude deep) at optical frequencies was postulated to be the effect of coating the water molecule with a highly resonant shell. Presently, we exploit the same concentric geometry for the formulation of an artificial dielectric. We derive the parameter dependence of the window formation that allows tailor-designing the novel structure according to prescribed specifications.

Without loss of generality, we perform the analysis for spherically shaped inclusions. The novel complex medium is an amorphous ensemble of spheres composed of a lossy core, coated with a highly resonant dielectric layer and embedded in a dielectric host. We study the resulting amorphous structure in the quasistatic regime where the size and spacing of the inclusions are smaller than the wavelength. For low-volume densities (filling

Manuscript received July 24, 1997; revised April 8, 1999.

C. A. Kyriazidou is with the Department of Electrical Engineering, University of California Los Angeles, Los Angeles, CA 90095 USA.

R. E. Diaz was with Northrop Grumman Corp., Chandler, AZ 85224 USA. He is now with the Department of Mechanical and Aerospace Engineering, Arizona State University, Tempe, AZ 85287-5306 USA.

N. G. Alexópoulos is with the Department of Electrical and Computer Engineering, University of California Irvine, Irvine, CA 92697 USA.

Publisher Item Identifier S 0018-926X(00)02623-5.

fraction <0.35), the analysis is based on the *classical theory of effective media* [13]–[16]. In this context, we demonstrate that the complex dielectric is a lossy substance over its entire spectrum except for the existence of *two* narrowband transparency windows, where it may be as lossless as desired.

We prove the existence of the windows, and specify analytically their exact location, shape, and depth within a four-decade spectrum. The parameter dependence of the window formation is explored and this allows, at least at the theoretical level, the prescription of constitutive materials and geometries needed for specific novel frequency selective media. In particular, for highly resonant shells, we observe a significant drop of five orders of magnitude or even larger in the bulk conductivity of the effective medium with respect to the core conductivity. This constitutes a transition from a metallic to a dielectric substance within the window range. The window bandwidth is adjustable according to the thickness of the coating layer. Bandwidths as narrow as 4–5% are possible for sufficiently thin layers. Moreover, the specification of the parameter dependence on the distance between the two windows allows the use of one or both of them according to application needs.

The proposed theoretical design is applicable from the microwave to the quasi-optical portion of the spectrum. Accordingly, we derive a general scale-independent discussion. For illustrative purposes we use a Lorentzian of quality $Q = 10^4$, representing an average, in orders of magnitude, of realizable Q values in the microwave and optical regimes.

The paper is organized as follows: Section II presents the novel dielectric design. Section II-A discusses physically realizable resonant dielectrics. Section II-B analyzes the low-density medium in terms of the effective medium theory. Section II-C contains the detailed physical characterization of the transparency windows. Section III refers to the implementation in the microwave region. Finally, Section IV contains a discussion of the results.

II. Novel Composite Dielectric

We examine an ensemble of spherical particles consisting of a lossy dielectric core coated with a highly resonant dielectric layer and embedded within a dielectric host. We consider the artificial dielectric within the quasistatic approximation, i.e., for wavelengths greater than the size and spacing of the individual implants. The layout of the mixture is shown in Fig. 1, where

$$\hat{\epsilon}_1 = \hat{\epsilon}_1^r - j\,\frac{\sigma_c}{\epsilon_0\omega},$$
$$\hat{\epsilon}_2 = 1 + \frac{\omega_p^2}{\omega_0^2 - \omega^2 + j\omega\Gamma}, \qquad \hat{\epsilon}_3 = \hat{\epsilon}_3^r \tag{1}$$

are the relative permittivities of the core, layer, and host dielectric, respectively. For most of this paper, we consider $\hat{\epsilon}_1^r = 1$ and $\hat{\epsilon}_3^r = 3$ (typical value of plastic dielectric), unless otherwise specified. The superscripts r and i denote the real and imaginary parts of complex quantities, respectively. $\sigma_c$is the conductivity of the core, while a and b denote the inner and outer radii of the coated spheres, respectively. The resonant material of the coating shell is characterized by its resonant frequency ω_0 the full-width at half maximum Γ and the plasma frequency ω_p.

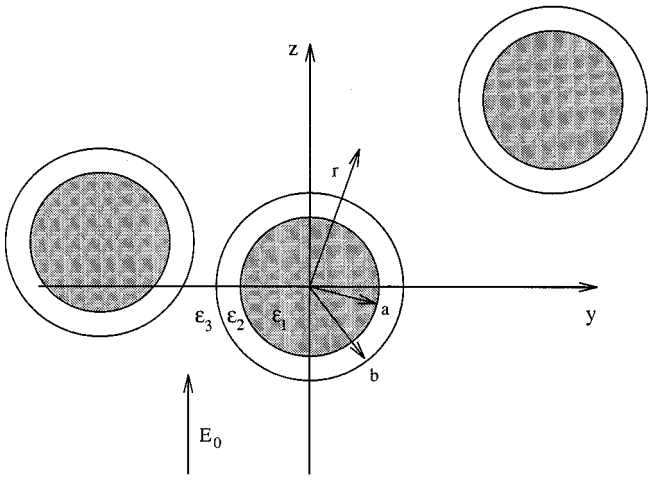

Fig. 1. Concentric geometry of inclusions.

There are two elements in the proposed composite that collaborate to create electromagnetic windows in the bulk. First, the choice of constitutive materials and, in particular, of the resonant dielectric whose dispersive behavior drives the dispersion of the composite. Second, the concentric geometry whose importance should not be underestimated. For instance, a dielectric loaded with plain spheres composed of a resonant dielectric will not perform the task. It is the use of the resonant dielectric precisely as a coating layer that results in transparency windows.

A. Resonant Dielectrics

This section discusses physically realizable resonant materials for use in coating the conducting spheres of the composite. In general, resonant dielectrics are described by relative permittivity functions of the form of $\hat{\epsilon}_2$ of (1). According to the classical Lorentz model, this dispersion naturally arises in harmonically bound systems that are also subject to damping [17]. A formally identical result for the permittivity arises from a precise quantum-mechanical description for the scattering of photons by atoms. Given the frequency dependence of $\hat{\epsilon}_2$, the Lorentzian dielectrics are characterized by a region of resonant absorption which, in natural dielectrics, usually occurs *at optical frequencies* due to rotations and vibrations of the atoms, ions or electrons.

In the microwave regime, possible candidates are macromolecules particularly engineered to slow down their physical rotational or vibrational modes. It should be emphasized that, although unusual, there exist physical systems with resonant frequencies as low as the microwave regime. Metal ammonia solutions constitute such examples with low-resonant frequency $\omega_0 \approx 10$ GHz due to relative large distances among charges and the relatively large masses of the charged particles [18]. This is of particular importance since it substantiates the realism and credibility of our theoretical design.

An accurate modeling of the dielectric behavior near 10 GHz, requires a multiple-oscillator model, reflecting the multiplicity

of physical oscillators in the solution [18]. Nonetheless, a single-oscillator model of the form

$$\hat{\epsilon}_L = 1 + \frac{\omega_p^2}{\omega_0^2 - \omega^2 + j\omega\Gamma},$$

with

$$\frac{1}{2\pi}\{\omega_0, \Gamma, \omega_p\} = \{9.5\ \text{GHz},\ 0.5\ \text{GHz},\ 57.66\ \text{GHz}\} \quad (2)$$

provides a reasonably good approximation. Fig. 2(a) depicts the fit of the very scant available data for the real part of the permittivity of Li–NH_3, shown by the dots, in terms of (2). In this manner indicative values of the Lorentzian parameters are deduced, while maintaining modeling simplicity. Although the windows created based on the data for Li–NH_3 are, at most, only one order of magnitude deep, as shown in Fig. 12, this is not necessarily the limit of the available performance with such natural materials. Moreover, the small number of data points available makes it difficult to ascertain the true number and magnitude of the Lorentzian terms constituting this resonance. The fact that the lowest frequency data point of the real part of the permittivity is so low in magnitude, yet less than a decade of frequency away from the resonance suggests that there may be Lorentzian components as sharp as the the one shown in Fig. 2(b), corresponding to

$$\frac{1}{2\pi}\{\omega_0, \Gamma, \omega_p\} = \{9.5\ \text{GHz},\ 0.05\ \text{GHz},\ 18.23\ \text{GHz}\} \quad (3)$$

where the same overall height for the imaginary peak is assumed as in (2). In general, physical resonances become typically sharper at higher frequencies, yielding deeper windows. For the rest of the paper, we discuss the proposed model within a normalized frequency range without restricting it to microwave frequencies.

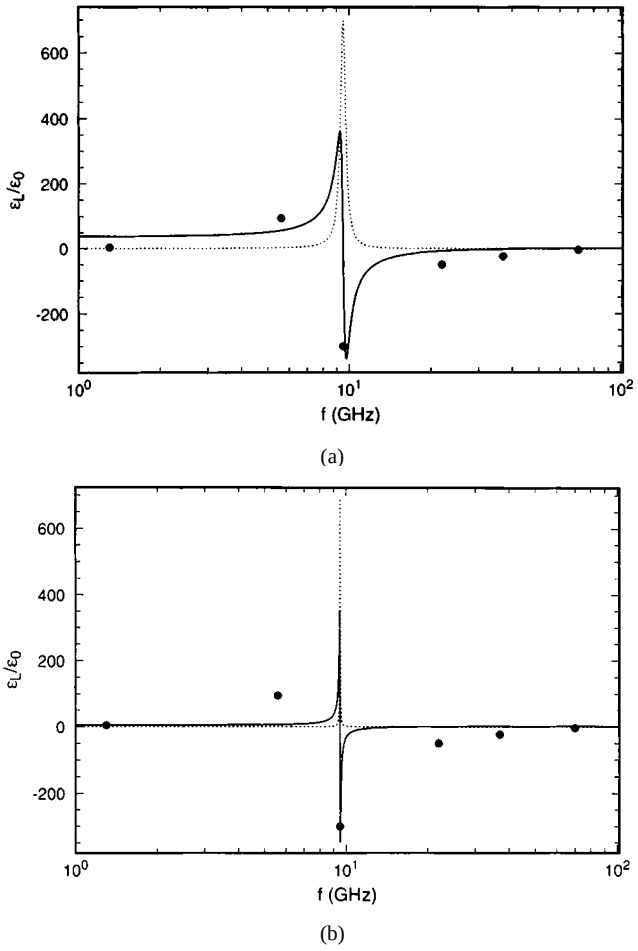

Fig. 2. Real (solid) and imaginary parts (dotted) of the single Lorentzian fit for the real permittivity data of Li–NH_3 represented by the dots: (a) Lorentzian of (2) and (b) Lorentzian of (3).

B. Effective Medium Analysis

This section sketches the derivation of the effective permittivity function of the composite medium within the range of validity of the classical theory of effective media, i.e., for low inclusion density, typically less than 0.35%. Accordingly, the electromagnetic response of artificial dielectrics is given within the framework of the point-dipole model. Implanted scatterers within a host medium of permittivity ϵ_3 acquire a dipole moment proportional to the value of the local field $\boldsymbol{E}$

$$\boldsymbol{p} = \epsilon_3\alpha(\boldsymbol{E}_0 + \boldsymbol{E}_{int}) = \epsilon_3\alpha\boldsymbol{E} \quad (4)$$

where α is the polarizability of the scatterer, $\boldsymbol{E}_0$ is the applied field and $\boldsymbol{E}_{int}$ is the interaction field, i.e., the field created by all other scatterers. Computation of $\boldsymbol{E}_{int}$ is the central problem in the theory of dielectrics. According to the classical theory applied here [21], the local field for spherical inclusions is

$$\boldsymbol{E} = \frac{\epsilon_{\text{eff}} + 2\epsilon_3}{3\epsilon_3}\boldsymbol{E}_0. \quad (5)$$

Since the polarization is also $\boldsymbol{P} = (\epsilon_{\text{eff}} - \epsilon_3)\boldsymbol{E}_0$, the effective permittivity of the composite is associated with the polarizability of individual inclusions according to the Maxwell Garnett equation (also known as the Clausius Mossotti equation) [19], [20]

$$\epsilon_{\text{eff}} = \epsilon_3\frac{1 + 2f_v\alpha'}{1 - f_v\alpha'} \quad (6)$$

where f_v is the volume fraction given in terms of the number density N of scatterers

$$f_v \equiv \frac{4\pi}{3}b^3N \quad (7)$$

and α' is the normalized polarizability of the inclusions defined as

$$\alpha' \equiv \frac{\alpha}{4\pi b^3}. \quad (8)$$

The static polarizability of the coated sphere is [17] (9), shown at the bottom of the next page, where $r_v \equiv (a/b)^3$ is the concentric volume ratio. Inputing this value into the Maxwell Garnett equation (6) yields the effective permittivity ϵ_{eff} for the composite. Consequently

$$\epsilon_{\text{eff}}^r = \epsilon_3\frac{(1 + 2f_v\alpha'^r)(1 - f_v\alpha'^r) - 2f_v^2(\alpha'^i)^2}{(1 - f_v\alpha'^r)^2 + (f_v\alpha'^i)^2} \quad (10)$$

$$\epsilon_{\text{eff}}^i = \epsilon_3\frac{3f_v\alpha'^i}{(1 - f_v\alpha'^r)^2 + (f_v\alpha'^i)^2}. \quad (11)$$

Casting the dispersive behavior of the composite in the form common for conducting dielectrics at microwave frequencies, its bulk conductivity is defined as

$$\sigma_{\text{bulk}} = \omega \epsilon^i_{\text{eff}}. \tag{12}$$

The parametric analysis of the transparency windows requires the real α'^r and imaginary α'^i parts of the polarizability, which, from (9), are given as

$$\alpha'^r \equiv \frac{\alpha^r}{4\pi b^3} = 1 - 3 \cdot \frac{(2 + r_v + (1 - r_v)E^r_{12})\Pi^r + (1 - r_v)E^i_{12}\Pi^i}{(\Pi^r)^2 + (\Pi^i)^2} \tag{13}$$

$$\alpha'^i \equiv \frac{\alpha^i}{4\pi b^3} = 3 \cdot \frac{(2 + r_v + (1 - r_v)E^r_{12})\Pi^i - (1 - r_v)E^i_{12}\Pi^r}{(\Pi^r)^2 + (\Pi^i)^2} \tag{14}$$

where we have defined

$$E^r_{12} - jE^i_{12} \equiv \frac{\epsilon_1}{\epsilon_2} = \frac{\epsilon^r_1\epsilon^r_2 + \frac{\sigma_c}{\omega}\epsilon^i_2}{(\epsilon^r_2)^2 + (\epsilon^i_2)^2} - j\frac{\epsilon^r_2\frac{\sigma_c}{\omega} - \epsilon^r_1\epsilon^i_2}{(\epsilon^r_2)^2 + (\epsilon^i_2)^2} \tag{15}$$

$$E^r_{23} - jE^i_{23} \equiv \frac{\epsilon_2}{\epsilon_3} = \frac{\epsilon^r_2}{\epsilon_3} - j\frac{\epsilon^i_2}{\epsilon_3} \tag{16}$$

$$\Pi^r \equiv 2(2 + r_v) + 2(1 - r_v)(E^r_{12} + E^r_{23}) + (1 + 2r_v)(E^r_{12}E^r_{23} - E^i_{12}E^i_{23}) \tag{17}$$

$$\Pi^i \equiv 2(1 - r_v)(E^i_{12} + E^i_{23}) + (1 + 2r_v)(E^i_{12}E^r_{23} + E^r_{12}E^i_{23}). \tag{18}$$

We examine the dispersive properties of the novel dielectric in general without restricting the discussion to a specific frequency range. To this effect, a natural choice of scale would involve the core conductivity, σ_c. In particular, the exact appropriate form chosen for the frequency normalization is

$$\omega_n = \sigma_c/\epsilon_0. \tag{19}$$

To illustrate the model performance we use a resonance with quality factor $Q = \omega_0/\Gamma = 10^4$ and parameters given as

$$\frac{1}{\omega_n}\{\omega_0, \Gamma, \omega_p\} = \{0.1,\ 10^{-5},\ 0.3162\}. \tag{20}$$

Although this Q value is higher than the corresponding ones for the Lorentzians of (2) and (3), it is still a moderate value, smaller by at least four orders of magnitude than corresponding Q values realized in atomic systems at high frequencies [21]. Fig. 3 presents the material response over four frequency decades

$$10^{-2} \ll \frac{\omega}{\omega_n} \ll 10^2 \tag{21}$$

indicating the lack of secondary grating lobes. In the limit $r_v \to 1$, the resonant shell disappears and the effective medium exhibits Debye-type permittivity [22], depicted in Fig. 3 with a dashed line. For coated implants the response consists of two localized disturbances on top of an otherwise Debye-type permittivity, shown in Fig. 3 with a solid line. Concerning the bulk conductivity of the effective medium, we observe a lossy dielectric except at the position of these resonances where narrow low-loss transparency windows appear. In the event of deep windows, as, for instance, in Fig. 3(c), where we have four orders of magnitude drop in the bulk conductivity, this region marks a transition from a medium of metallic nature to a dielectric substance. It should be noted that for a nonresonant dielectric coating the effective medium exhibits only a Debye-type permittivity, indicating that the windows are essentially driven by the resonant Lorentzian dielectric. On the other hand, the molding of the disturbance in the desired form of a window is due to the use of the Lorentzian medium as a coating in a concentric geometry.

C. Characteristics of Transparency Windows

Before embarking into the parametric characterization of the windows in terms of width, depth and location, it is worthwhile to discuss the physical mechanisms causing the transparency. In general, the absorption efficiency of a small sphere is proportional to the imaginary part of its polarizability [17] and, thus, we expect transparency at frequencies where $\text{Im}(\alpha')$ is minimum. It is useful to define a plain spherical implant equivalent to the coated one by virtue of having the same polarizability. Its equivalent permittivity is defined by

$$\alpha' = \frac{\frac{\epsilon_{eq}}{\epsilon_3} - 1}{\frac{\epsilon_{eq}}{\epsilon_3} + 2} \tag{22}$$

where α' is given in (8) and (9). Fig. 4(a) and (b) presents the equivalent permittivity function and the imaginary part of the polarizability $\text{Im}(\alpha')$ in the window regions. On the one hand, the left window is located precisely at the position where ϵ_{eq} exhibits a phase transition driven by the Lorentzian permittivity. On the other hand, the right window is characterized by ϵ^r_{eq}, $\epsilon^i_{eq} \approx 0$, indicating that the metallic nature of the core is completely screened and the coated sphere behaves as a low-loss dielectric with dielectric function less than unity. Mathematically speaking, the transparency window locations will be identified

$$\alpha = 4\pi b^3 \left(1 - \frac{3\left(2 + r_v + (1 - r_v)\frac{\epsilon_1}{\epsilon_2}\right)}{\left(2 + \frac{\epsilon_1}{\epsilon_2}\right)\left(2 + \frac{\epsilon_2}{\epsilon_3}\right) + 2r_v\left(1 - \frac{\epsilon_1}{\epsilon_2}\right)\left(1 - \frac{\epsilon_2}{\epsilon_3}\right)} \right) \tag{9}$$

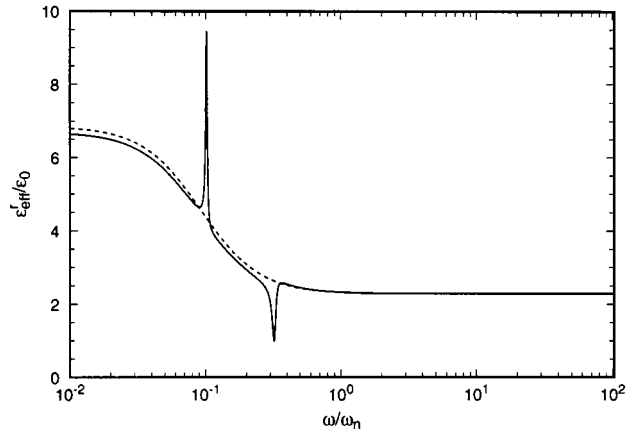

(a)

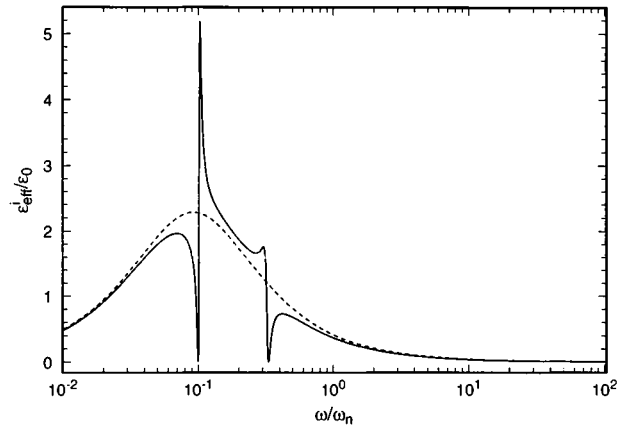

(b)

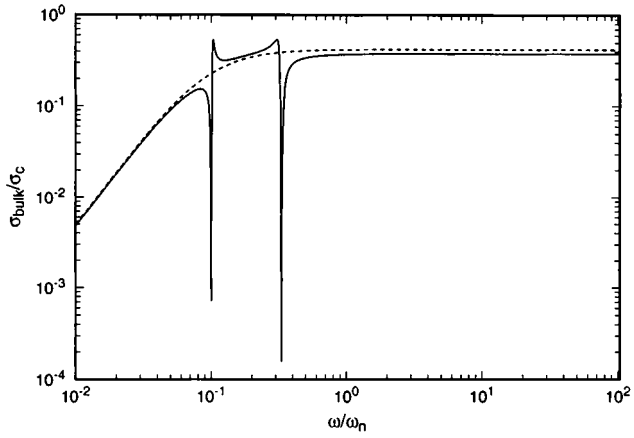

(c)

Fig. 3. Dispersive properties of effective medium with coated (solid) and uncoated (dashed) inclusions for $f_v = 0.3$, $r_v = 0.9$, $\omega_0/\omega_n = 0.1$, $\Gamma/\omega_n = 10^{-5}$, $\omega_p/\omega_n = 0.3162$: (a) real part of effective permittivity, (b) imaginary part of effective permittivity, and (c) bulk conductivity.

below as the frequency where the real part of the Lorentzian permittivity $\hat{\epsilon}_2^r$ vanishes.

This equivalent picture for the implant also helps in justifying the surface modes which are manifested at the band edge of the left transparency band. These are electromagnetic modes characteristic of small particles, associated with the vanishing

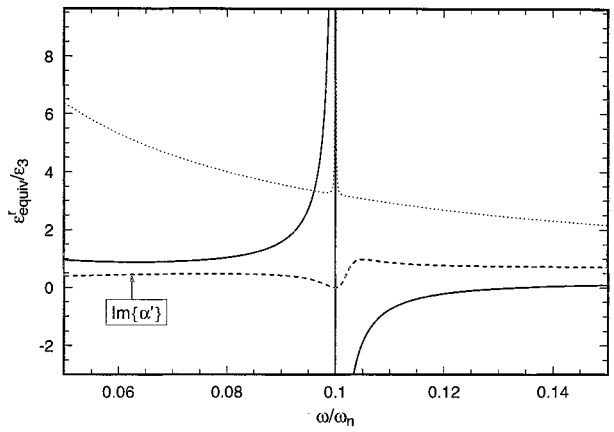

(a)

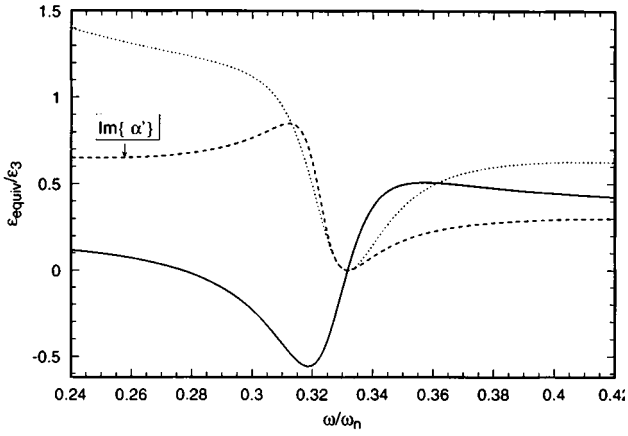

(b)

Fig. 4. Real (solid) and imaginary (dotted) parts of ϵ_{eq}/ϵ_3 and $\mathrm{Im}(\alpha')$ (dashed) in window regions.

of denominators in certain expansion coefficients of the Mie series representing the wave scattered by a small spherical particle [17]. In this manner, resonant modes arise whereby the field inside the spherical scatterer is highly localized near its surface, accompanied by high absorption. Although dynamic in nature, surface modes effects may be explained in electrostatic terms. The condition for excitation of the first-order surface mode in a small sphere is derived from the sphere polarizability α in the form

$$\alpha^{-1} = 0 \quad \text{or} \quad \epsilon_1 = -2\epsilon_h \tag{23}$$

where ϵ_1, ϵ_h are the dielectric functions of the sphere and host, respectively. In general, for coated spherical implants the condition for surface modes is the vanishing of the denominator of the polarizability given in (9). In our case, however, singularities appear also in the numerator and, thus, we have to examine the issue in terms of the equivalent permittivity. Thus, the condition for surface modes becomes

$$\frac{\epsilon_{eq}}{\epsilon_3} \approx -2. \tag{24}$$

This is approximately true near the left window band edge where $\mathrm{Im}(\epsilon_{eq}/\epsilon_3)$ is small, as shown in Figs. 4(a) and 5. According to [17], surface plasmons are not examples of failure of the bulk

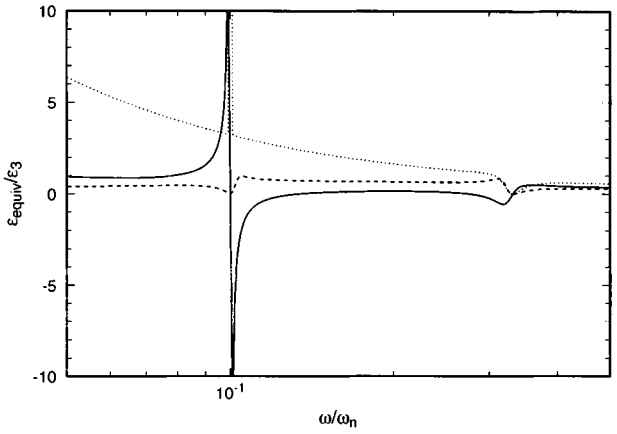

Fig. 5. Real (solid) and imaginary (dotted) parts of ϵ_{eq}/ϵ_3 and $\mathrm{Im}(\alpha')$ (dashed) overall the spectrum.

dielectric constant to be applicable to small particles. Thus, the quasistatic prediction is still valid in the surface mode region and dynamic phenomena may be neglected.

The parametric characterization of the windows is best carried out using the closed form for the permittivity of (6). However, this is a complicated function of the frequency, which forbids a straightforward treatment through differentiation with respect to ω and requires a different approach. As mentioned above, the overall dispersion of the composite may be seen as a superposition of a resonant and a Debye-type behavior. Thus, the parametric analysis may be performed analytically based on the localized properties of the Lorentzian resonance, as specified in $\hat{\epsilon}_2^r(\omega)$ and $\hat{\epsilon}_2^i(\omega)$, given in (1). These are functions of narrow support and, according to the distribution theory in functional analysis, they are representations of a Dirac δ-function. Thus, we may write [23] for $\omega\Gamma \ll 1$

$$\hat{\epsilon}_2^i(\omega) = \frac{\omega_p^2 \omega \Gamma}{(\omega_0^2 - \omega^2)^2 + \omega^2 \Gamma^2} \approx \omega_p^2 \pi \delta(\omega^2 - \omega_{r1}^2) \tag{25}$$

where

$$\omega_{r1} \equiv \sqrt{\omega_0^2 - \Gamma^2/4} \approx \omega_0 \tag{26}$$

is the location of the maximum in $\hat{\epsilon}_2^i$.

Outside the Lorentzian resonant region, the effective permittivity of the composite is a function of two small parameters $\hat{\epsilon}_2^r$ and $\hat{\epsilon}_2^i$. Since $\hat{\epsilon}_2^i$ is negligible, by setting it equal to zero we examine ϵ_{eff} exclusively as a function of $\hat{\epsilon}_2^r$. From (13)–(18) we have

$$\Pi^r = 2(2 + r_v) + 2(1 - r_v)\left(\frac{\epsilon_1^r}{\epsilon_2^r} + \frac{\epsilon_2^r}{\epsilon_3}\right) + (1 + 2r_v)\frac{\epsilon_1^r}{\epsilon_3} \tag{27}$$

$$\Pi^i = \left(2(1 - r_v)\frac{1}{\epsilon_2^r} + (1 + 2r_v)\frac{1}{\epsilon_3}\right)\frac{\sigma_c}{\omega} \tag{28}$$

$$\alpha'^r = 1 - 3\frac{\left(2 + r_v + (1 - r_v)\epsilon_1^r \dfrac{1}{\epsilon_2^r}\right)\Pi^r + (1 - r_v)\dfrac{\sigma_c}{\omega}\dfrac{1}{\epsilon_2^r}\Pi^i}{(\Pi^r)^2 + (\Pi^i)^2} \tag{29}$$

$$\alpha'^i = 3\frac{\left(2 + r_v + (1 - r_v)\epsilon_1^r \dfrac{1}{\epsilon_2^r}\right)\Pi^i - (1 - r_v)\dfrac{\sigma_c}{\omega}\dfrac{1}{\epsilon_2^r}\Pi^r}{(\Pi^r)^2 + (\Pi^i)^2}. \tag{30}$$

It follows that ϵ_{eff} is essentially a function of the real Lorentzian permittivity and its inverse, i.e., $\epsilon_{\text{eff}} = f(\omega, \hat{\epsilon}_2^r(\omega), (\hat{\epsilon}_2^r(\omega))^{-1})$. Consequently, it is a smooth Debye-type function, except at the extrema and singularities of the Lorentzian functions $\hat{\epsilon}_2^r(\omega), (\hat{\epsilon}_2^r(\omega))^{-1}$, which themshelves have constant values except for a small region where they vary violently.

Thus, we proceed to specify the window position semi-analytically in two steps. First, we study analytically $\hat{\epsilon}_2^r(\omega)$ and $(\hat{\epsilon}_2^r(\omega))^{-1}$ and locate the extrema and singularities. Second, we examine numerically ϵ_{eff} in these positions, along with the previously excluded ω_0 region in order to identify its local extrema. In this manner, two regions of interest emerge, each corresponding to a transparency window.

1) The *region around* ω_0 corresponding to the position of the left window. For $\Gamma \ll 1$, this is the accumulation region for

$$\hat{\epsilon}_2^r(\omega) - \text{extrema: } \omega_{r2}^{\pm} = \left(\omega_0^2 + \frac{\Gamma^2}{2} \pm \Gamma\sqrt{\omega_0^2 + \frac{\Gamma^2}{4}}\right)^{1/2} \approx \omega_0 \tag{31}$$

$$(\hat{\epsilon}_2^r(\omega))^{-1} - \text{extrema: } \omega_{r3}^{\pm} = \omega_0\sqrt{1 \pm \frac{\Gamma}{\omega_0}} \approx \omega_0 \tag{32}$$

$$(\hat{\epsilon}_2^r(\omega))^{-1} - \text{singularity: } \omega_{s1} = \omega_0\left(1 + \frac{\omega_p^2 - \Gamma^2}{2\omega_0^2} - \frac{\omega_p^2 - \Gamma^2}{2\omega_0^2}\sqrt{1 - \frac{4\Gamma^2\omega_0^2}{(\omega_p^2 - \Gamma^2)^2}}\right)^{1/2} \approx \omega_0\sqrt{1 + \frac{\Gamma^2}{\omega_p^2}} \approx \omega_0. \tag{33}$$

2) The *region around* ω_{s2} corresponding to the right window. This is the location of the singularity

$$(\hat{\epsilon}_2^r(\omega))^{-1} - \text{singularity: } \omega_{s2} = \omega_0\left(1 + \frac{\omega_p^2 - \Gamma^2}{2\omega_0^2} + \frac{\omega_p^2 - \Gamma^2}{2\omega_0^2}\sqrt{1 - \frac{4\,\Gamma^2\omega_0^2}{(\omega_p^2 - \Gamma^2)^2}}\right)^{1/2} \approx \omega_0\sqrt{1 + \frac{\omega_p^2}{\omega_0^2}}. \tag{34}$$

Thus, we conclude that the window minima are positioned at

$$\omega_{\text{left}} = \omega_0, \quad \omega_{\text{right}} = \omega_{s2} \approx \omega_0\sqrt{1 + \frac{\omega_p^2}{\omega_0^2}} \tag{35}$$

which are depicted by dots in Fig. 6(a) and (b), respectively. These values approach the actual minima with an accuracy of the order of 10^{-6}. The small offset in the position of minimum for the right window with respect to ω_{right} is due to the fact that $\hat{\epsilon}_2^i$ in our previous analysis is a very small number but not exactly zero. The distance among windows depends exclusively on the Lorentzian parameters and mainly on ω_p^2/ω_0^2. For increasing values of this parameter, the singularity ω_{s2}, in accord with the right window, slide to the right, as shown in Fig. 7.

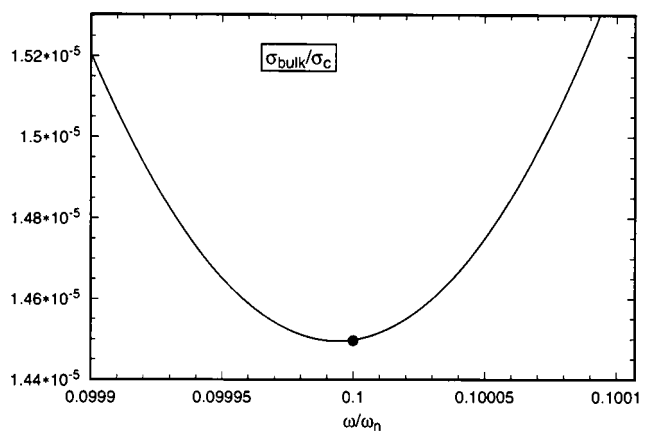

(a)

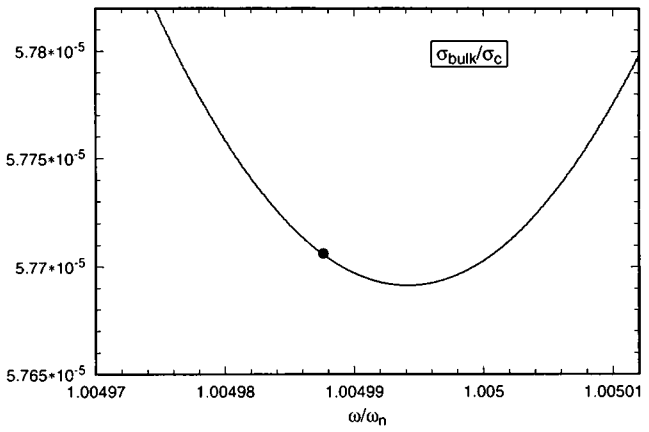

(b)

Fig. 6. $\sigma_{\rm bulk}/\sigma_c$ for composite with $f_v = 0.1$, $r_v = 0.9$, $\omega_0/\omega_n = 0.1$, $\Gamma/\omega_n = 10^{-5}$, $\omega_p/\omega_n = 1.0$ in: (a) left and (b) right windows and location of window minima from (35), indicated by the dots.

Given their locations, the window minima may be found analytically

$$\left[\frac{\sigma_{\rm bulk}}{\sigma_c}\right]_{\rm min} = \left|\frac{\sigma_{\rm bulk}}{\sigma_c}(\omega)\right|_{\omega=\omega_{\rm left},\omega_{\rm right}}. \qquad (36)$$

For the sharp resonance shown in Fig. 6(a) and (b), we observe five orders of magnitude drop in the conductivity of the composite with respect to the core conductivity.

The window depth may be defined as the bulk conductivity normalized to the conductivity of the high frequency plateau $\omega \to \infty$

$$\text{Window Depth} = \frac{\sigma_{\rm bulk}(\omega = \omega_{\rm left,right})}{\sigma_{\rm bulk}(\omega \to \infty)}. \qquad (37)$$

The variation of window minima (36) and window depth (37), with respect to the concentric volume ratio, $r_{\rm v}$, and to the filling fraction f_v are depicted in Figs. 8 and 9, respectively. According to Fig. 8, the values of window minima [curves denoted by (a)] and depth [curves denoted by (b)] increase (windows become more shallow) for thinning coating shell and the window disappears in the limit $r_v \to 1$. Fig. 9 reveals a different behavior for increasing f_v depending on the normalization of the bulk conductivity: The value of window minima [curves denoted by (a)] increase, while the value of window depth [curves denoted

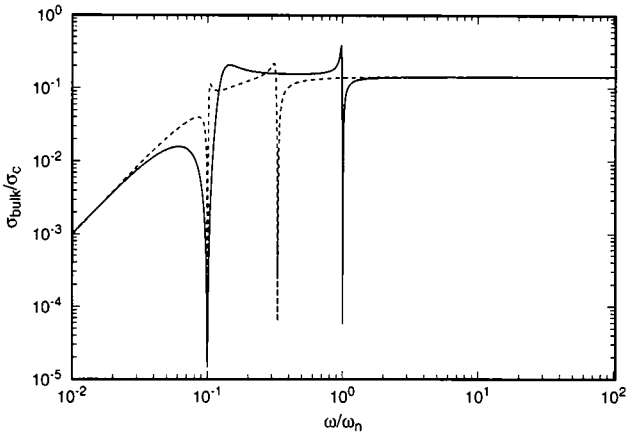

Fig. 7. Bulk conductivity of effective medium with $f_v = 0.1$, $r_v = 0.9$, $\omega_0/\omega_n = 0.1, \Gamma/\omega_n = 10^{-5}$. Relative positioning of windows for $\omega_p/\omega_n = 0.3162$ (dashed) and $\omega_p/\omega_n = 1.0$ (solid).

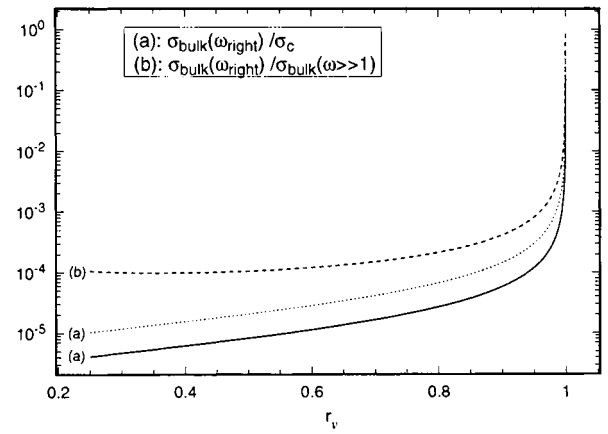

Fig. 8. (a) Window minimum and (b) window depth for right window as a function of the coating thickness r_v for composite with $\omega_0/\omega_n = 0.1, \Gamma/\omega_n = 10^{-5}$, $\omega_p/\omega_n = 1.0$. Window minima depicted for $f_v = 0.1$ (solid) and $f_v = 0.3$ (dotted). Window depth plotted for $f_v = 0.1$ (dashed).

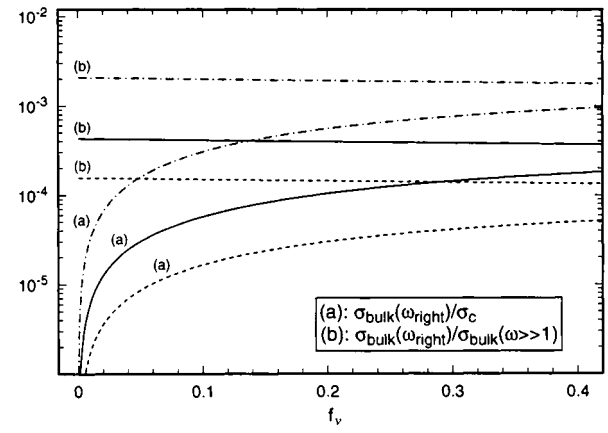

Fig. 9. (a) Window minimum and (b) window depth for right window as a function of filling fraction f_v for composite with $r_v = 0.7$ (dashed), 0.9 (solid), 0.98 (dashed-dotted) and $\omega_0/\omega_n = 0.1, \Gamma/\omega_n = 10^{-5}, \omega_p/\omega_n = 1.0$.

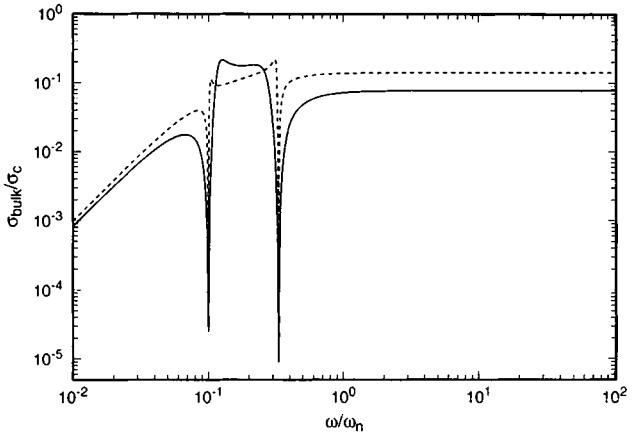

(a)

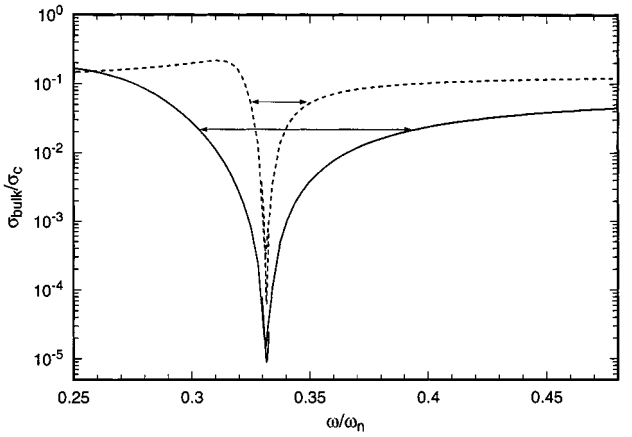

(b)

Fig. 10. Bulk conductivity in: (a) overall spectrum and (b) right window, for composite with $r_v = 0.9$ (dashed) to $r_v = 0.7$ (solid) and $f_v = 0.1, \omega_0/\omega_n = 0.1, \Gamma/\omega_n = 10^{-5}, \omega_p/\omega_n = 0.3162$.

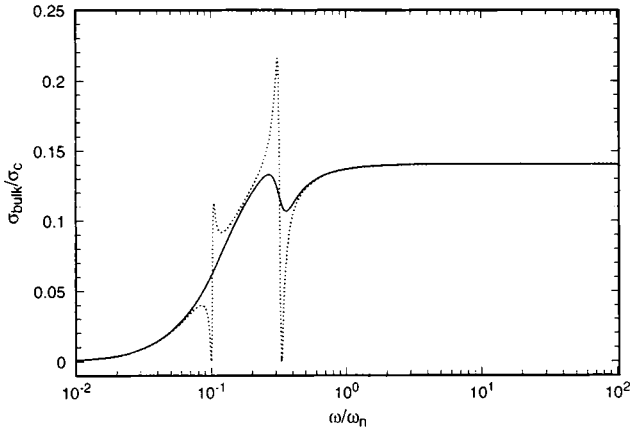

(a)

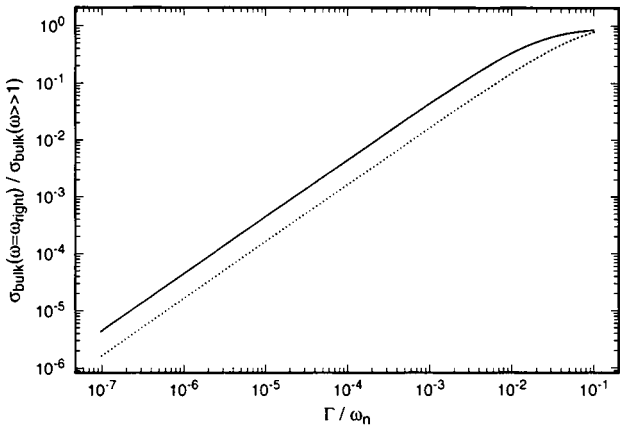

(b)

Fig. 11. Window formation for composite with $f_v = 0.1, \omega_0/\omega_n = 0.1, \omega_p = 0.3162$: (a) bulk conductivity for $r_v = 0.9$ and $\Gamma/\omega_n = 10^{-5}$ (dotted), $\Gamma/\omega_n = 10^{-1}$ (solid) and (b) right window depth as a function of Γ/ω_n for $r_v = 0.9$ (solid) and $r_v = 0.7$ (dotted).

by (b)] slightly decrease. The latter indicates that the window does not become drastically deeper with increasing filling fraction but depth may increase by a factor of two or three.

The window bandwidth may be defined as the ratio of the full width at half-minimum over the center frequency. The most significant parameter affecting it is the thickness of the coating layer, which is a geometrical element and thus easily controlled in manufacturing. As shown in Fig. 10, the bandwidth decreases (narrower windows) with increasing r_v, i.e., with thinner shell. In particular, a thin layer of $r_v = 0.9$ corresponds to a bandwidth of 7.5% and may be further diminished by decreasing the layer thickness. For a thick layer of $r_v = 0.7$ the bandwidth increases to 25%. On the other side, an increase in the filling fraction variation causes only a slight increase in the bandwidth [compare Figs. 3(c) and 7].

The effects of the Lorentzian parameters ω_0, ω_p on the window formation were discussed previously: ω_0 specifies the location of the left window in the effective medium, allowing it to slide toward or away from the plateau. ω_p determines the distance among windows so that one or both windows remain within the bandwidth of interest. The width Γ, which controls the sharpness of the Lorentzian resonance, directly influences the window depth and bandwidth, as shown in Fig. 11(a). Windows deepen for sharper Lorentzian resonances, increasing Γ's, according to Fig. 11(b).

III. Implementation in the Microwave Regime

Application of the design at microwave frequencies requires both the background Debye process as well as the Lorentzian superposition to occur at those frequencies. The Debye relaxation frequency for metallic spheres of conductivity σ immersed within a dielectric host is given by

$$\omega_{\text{relax}} \approx \frac{\sigma}{3\epsilon_0}. \tag{38}$$

For $\sigma_c = 8$ Siemens/m, the Debye relaxation appears approximately at 10 GHz. Introducing the Lorentzian forms (2) and (3) that fit the Li–NH_3 data, we obtain a response depicted in Fig. 12. Although the windows created here are one to two orders of magnitude deep, the performance will improve for resonant media of higher quality. The plateau conductivity itself is given by the background Debye process, describing the mixture of metallic spheres within a dielectric host. Thus, it depends on σ_c and f_v. Obviously, for lower σ_c, both windows of Fig. 12

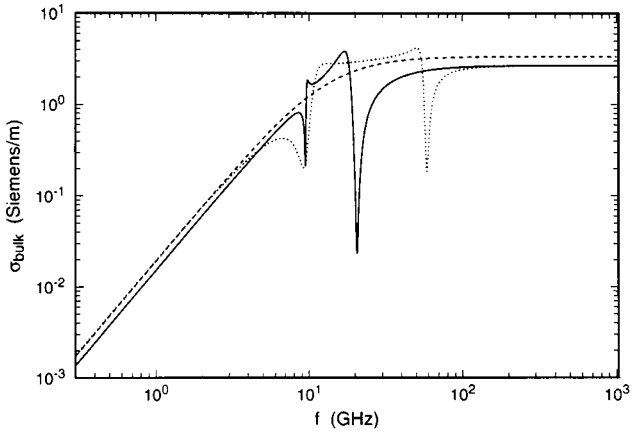

Fig. 12. Bulk conductivity of effective medium with $f_v = 0.3$, $r_v = 0.8$, $\sigma_c = 8$ Siemens/m, for plain uncoated sphere (dashed) for sphere coated with Lorentzian of (2) (dashed) and sphere coated with Lorentzian of (3) (solid).

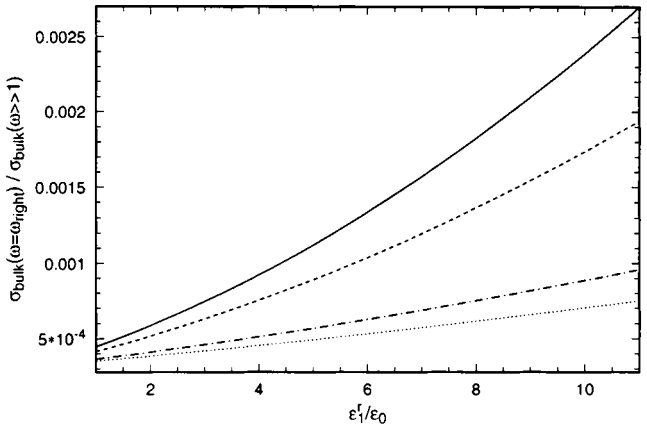

Fig. 13. Right window depth as a function of the core permittivity $\hat{\epsilon}_1^r$ for composite with $\omega_0/\omega_n = 0.1, \Gamma/\omega_n = 10^{-5}, \omega_p/\omega_n = 0.3162$. For $\epsilon_3 = 3$, the solid and dashed lines correspond to $f_v = 0.1$ and $f_v = 0.3$, respectively. For fixed $f_v = 0.1$, the dashed–dotted line and dotted lines correspond to $\hat{\epsilon}_3 = 13$ and $\hat{\epsilon}_3 = 30$, respectively.

move further to the right in the plateau, which levels off earlier and at a lower value.

To comply with the assumptions underlying the effective medium analysis, it is necessary that the size of the spherical implants and their coatings is significantly small, of the order of micrometers for the microwave and millimeter-wave regimes or of the order of nanometers for the quasioptical region. This does not pose a fabrication issue, since existing nano-technology creates submicrometer particles in the form of microballoons or coated and plain microspheres [17], [24]–[26]. Concerning the issue of applicability of bulk optical constants to such small particles, good agreement has been observed for particles in the size range of 3–4 nm [17].

Up until now, we have assumed that the relative dielectric constant of the core and host are $\hat{\epsilon}_1^r = 1$ and $\epsilon_3^r = 3$ (typical value for plastic dielectrics), respectively. The low-core conductivity at microwave frequencies, below that of pure carbon, implies a composite material which in general possesses a real part of permittivity $\hat{\epsilon}_1^r$ greater than one. Thus, it is important to examine the dependence on the type of materials used for the core and host. In Fig. 13 we observe a dramatic decrease in depth for increasing $\hat{\epsilon}_1^r$. However, as the dotted plots in this same figure show, an increase in the host medium permittivity counteracts that effect and there remains a substantial window depth. This effect is also produced through an increase in the filling fraction f_v, as the dashed plot of Fig. 13 indicates.

IV. Discussion

We have presented a method of creating frequency selectivity from bulk composite matter based on the geometry and the resonant properties of the constituents. We have illustrated the approach by presenting the theoretical design of a complex medium consisting of spherical inclusions coated with a highly resonant shell and implanted within a dielectric host. This novel medium exhibits frequency selective properties in the form of two narrowband transparency windows over a four-decade spectrum. The presented analysis allows full control over the window properties by manipulating the geometry and choosing the materials used for the inclusions. In this sense, we are able to achieve optimization of the window design with respect to their placement within the spectrum toward or away from the plateau appearing at large frequencies, the distance among them, their depth and bandwidth.

The present work motivates research in the development and synthesis of Lorentzian resonant dielectrics for use as implant coatings, thus driving the frequency dispersion of the mixture. In fact, the position and sharpness of these resonances directly reflect the position and depth of the two transparency windows in the effective medium. Thus, sharp resonances at a variety of positions are required in order to form the necessary ingredients for the construction of this novel class of media to be used for the coating layer. Such highly resonant media exist in nature, for instance, the ammonia molecule in the millimeter wave region, the iodine in the blue spectrum of the optical frequencies, MgO in the visible regime, and α-SiC in the far infrared spectrum [17]. In particular, we have discussed metal-ammonia solutions which resonate at approximately 10 GHz, thus adding practical credibility to our theoretical design in the microwave regime. Although we do not mention specific manufacturing procedures for the implants and the overall composite, this is not an issue since existing nanotechnology is able to construct plain and coated microspheres of the order of nanometers using a variety of materials.

The geometrical properties of the structure have also significant effects on the window formation, providing considerable control in manufacturing. The depth of the window increases for increasing filling fraction and this motivates an extension of the present analysis beyond the effective media theories, to denser materials up to the limit of almost touching spherical inclusions [27]. A more dramatic change in the window depth appears with the variation in the ratio of the inner to total spherical volumes, r_v, where a span of many orders of magnitude is possible, as indicated by Fig. 8. In fact, both depth and width of the transparency windows increase independently for thicker coating layers, thus allowing the exact formation of windows according to almost arbitrary specifications. To put it differently, the larger the resonant shell, the larger the windows and, in fact,

it seems beneficial to use the right-side window since it is always closer to the plateau and, in general, deeper. In addition, given that the distance among the two transparency windows is controllable, extremely narrow passband and stop-band filters are possible.

REFERENCES

[1] T. A. Cwik and R. Mittra, "Scattering from general periodic screens," *Electromagn.*, vol. 5, no. 4, p. 263, Dec. 1985.

[2] B. A. Munk, R. G. Kouyoumjian, and L. Peters Jr., "Reflection properties of periodic surfaces of loaded dipoles," *IEEE Trans. Antennas Propagat.*, vol. AP-19, p. 612, Sept. 1971.

[3] S. W. Schneider and B. A. Munk, "The scattering properties of 'super dense' arrays of dipoles," *IEEE Trans. Antennas Propagat.*, vol. 42, p. 463, Apr. 1994.

[4] J.-O. Ousbeck and L. Petterson, "Frequency selective radomes," in *Proc. 3rd Int. Conf. Electromagn. Aerosp. Applicat.*, Torino, Italy, Sept. 1993, p. 115.

[5] B. Philips, E. A. Parker, and R. J. Langley, "Curved dipole frequency selective surfaces," in *Proc. 3rd Int. Conf. Electromagn. Aerosp. Applicat.*, Torino, Italy, Sept. 1993, p. 123.

[6] R. J. Langley and C. K. Lee, "Design of single-layer frequency selective surfaces for multiband reflector antennas," *Electromagn.*, vol. 5, no. 4, p. 331, 1985.

[7] D. Bresciani and S. Contu, "Scattering analysis of dichroic subreflectors," *Electromagn.*, vol. 5, no. 4, p. 375, 1985.

[8] M. S. Durschlag and T. A. DeTemple, "Far-IR optical properties of freestanding and dielectrically backed metal meshes," *Appl. Opt.*, vol. 20, no. 7, p. 1245, Apr. 1981.

[9] E. J. Danielewicz and P. D. Coleman, "Hybrid metal mesh-dielectric mirrors for optically pumped far-infrared lasers," *Appl. Opt.*, vol. 15, no. 3, p. 761, Mar. 1976.

[10] C. M. Horwitz, "A new solar selective surface," *Opt. Commun.*, vol. 11, no. 2, p. 210, June 1974.

[11] W. A. Janos, "Synthetic dielectric material for broadband-selective absorption and reflection," in *IEEE AP-S Int. Symp. Dig.*, Newport Beach, CA, June 1995, U.S. Patent 5 298 903, Mar. 1994, pp. 1852–1855.

[12] R. E. Diaz and N. G. Alexópoulos, "An analytic continuation method for the analysis and design of dispersive materials," *IEEE Trans. Antennas Propagat.*, vol. 45, p. 1602, Nov. 1997.

[13] C. J. F. Bottcher, *Theory of Electric Polarization*. New York: Elsevier, 1952, pp. 199–212, 417.

[14] G. A. Niklasson, C. G. Granqvist, and O. Hunderi, "Effective medium models for the optical properties of inhomogeneous media," *Appl. Opt.*, vol. 20, p. 26, 1981.

[15] H. Looyenga, "Dielectric constants of heterogeneous mixtures," *Physica*, vol. 31, p. 401, 1965.

[16] L. D. Landau and E. M. Lifshitz, *Electrodynamics of Continuous Media*, 2nd ed. New York: Pergamon Press, 1960, p. 45.

[17] C. F. Bohren and D. R. Huffman, *Absorption and Scattering of Light by Small Particles*. New York: Wiley, 1983, ch. 9, sec. 5.2, 12.1, 12.3, 12-4, 9.1.4, 9.1.5, p. 149.

[18] K. G. Breitschwerdt and H. Radscheit, "Microwave resonant absorption in metal-ammonia solutions," *Phys. Lett.*, vol. 50A, no. 6, p. 423, Jan. 1975.

[19] J. C. M. Garnett, "Colors in metal glasses and in metallic films," *Phil. Trans. Roy. Soc. London*, vol. 203, p. 385, 1904.

[20] ——, "Colors in metal glasses and in metallic films," *Phil. Trans. Roy. Soc. London*, vol. 203, p. 385, 1904.

[21] A. R. von Hippel, *Dielectrics and Waves*. New York: Wiley, 1954, pp. 97–98, 166–169.

[22] P. Robert, *Electrical and Magnetic Properties of Materials*. Norwood, MA: Artech House, 1988, pp. 317–325.

[23] G. Arfken, *Mathematical Methods for Physicists*, 3rd ed. New York: Academic, 1985, p. 488.

[24] M. L. Gorodetsky, A. A. Savchenkov, and V. S. Ilchenko, "Ultimate Q of optical microsphere resonators," *Opt. Lett.*, vol. 21, no. 7, p. 453, Apr. 1996.

[25] I. W. Hall and C. Poteet, "High strain rate and other properties of a carbon microsphere reinforced magnesium alloy," *J. Mater. Sci. Lett.*, vol. 15, no. 12, p. 1015, June 1996.

[26] T. Tani, K. Takatori, N. Watanabe, and N. Kamiya, "Metal oxide powder synthesis by the emulsion combustion method," *J. Mater. Res.*, vol. 13, no. 5, p. 1099, May 1998.

[27] C. A. Kyriazidou, R. E. Diaz, and N. G. Alexópoulos, "Rayleigh analysis of novel dense medium exhibiting narrowband transparency window," in *Conf. Proc. 14th Annu. Rev. Progress Appl. Computat. Electromagn.*. Monterey, CA, Mar. 1998, p. 179.

Chryssoula A. Kyriazidou (M'98) received the B.S. degree in physics from the University of Athens, Greece, in 1984, and the M.S. and Ph.D. degrees in physics from the University of Michigan, Ann Arbor, in 1989 and 1992, respectively. She is currently working toward the Ph.D. degree in electrical engineering at the University of California, Los Angeles.

She worked as a Postdoctoral Research Associate with the High Energy Physics Group at Brookhaven National Laboratory from 1992 to 1993 and at Argonne National Laboratory from 1993 to 1996. Her research then included quantum field theory with an emphasis on quantum radiative corrections to electroweak scattering processes. She has authored 15 publications in the area of electromagnetics. Her current research interests include novel composite materials, photonic bandgap structures, novel antenna design and monolithics microwave integrated circuits (MMIC's), accelerated full-wave codes for electromagnetic simulations, and signal propagation in urban media.

Rodolfo E. Diaz, was born in Santurce , Puerto Rico. He received the B.S. degree in physics from Yale University, New Haven, CT, and the M.S. (physics) and the Ph.D. (electrical engineering) degrees from University of California at Los Angeles (UCLA) in 1978, 1980, and 1992, respectively.

During his 20 years in the aerospace industry, his work has spanned many of the disciplines comprising modern electromagnetic engineering. From 1978 to 1983 he was at Rockwell International, Space Division, working on Lightning Protection, Electromagnetic Compatibility, and electromagnetic radiation safety on the Space Shuttle. Form 1983 to 1988 he worked at Ford Aerospace in the Missile Systems Organization on the design of novel stripline components, microwave lenses, high-temperature broad-band radomes, and absorber materials for broad-band antennas. In 1988 he joined Hexcel Corporation's Advanced Products Division subsequently acquired in 1995 by Northrop Grumman Corporation, where he led the design, evaluation and prototyping of electromagnetic composite materials for low-observable applications. He is currently at Arizona Stae University. He holds nine patents ranging form the design of broad-band radomes to the amplification of magnetic fileds.

Nicólaos G. Alexópoulos, (S'68–M'69–SM'82–F'87) was born in Athens, Greece, on April 14, 1942. He received the degree from the Eighth Gymnasium of Athens, Greece, in 1959, and the B.S.E.E., M.S.E.E., and Ph.D. degrees from the University of Michigan, Ann Arbor, in 1965, 1967, and 1968, respectively.

He joined the School of Engineering and Applied Science at the University of California, Los Angeles (UCLA), where he was a member of the faculty of the Electrical Engineering Department from 1969 to 1996. While at UCLA he served as Associate Dean of Faculty Affairs from 1986 to 1987 and Chair of the Electrical Engineering Department from 1987 to 1992. Since January 1997 he has been a Professor of the Electrical and Computer Engineering Department at the University of California, Irvine, where he also serves as the Dean of the School of Engineering. He has served over the years as a Consultant to a variety of U.S. and foreign corporations and the U.S. Government. In addition, he has been on the editorial board of various professional journals and, more recently, he served as Editor-in-Chief of *Electromagnetics*. He is the author of over 250 refereed jounal and conference proceedings papers. His recent research activities have focused on the modeling and design of three-dimensional integrated circuits and printed antennas in multilayered materials, wireless communication antennas and systems, interconnect problems in complex networks, novel materials and smart structures in low-observable systems, and computational methods.

Dr. Alexopulos was corecipient of the IEEE (Institute of Electrical and Electronic Engineers) S. E. Schelkunoff Prize Best Paper Award in 1985 and 1998.